

The model and extra friction term effects in standard siren simulation

Xianfu Su¹, Dongze He¹ and Yi Zhang^{a,1}

¹Chongqing University of Posts and Telecommunications, Chongqing 400065, China

Received: date / Accepted: date

Abstract To investigate the model and extra friction term effects in standard siren (SS) data simulation of modified gravity, we simulated three types of SS data based on different fiducial models which are Λ CDM, $f(Q)|_{PE}$ and $f(Q)|_{HT}$ models. The current cosmological electromagnetic (EM) observations are combined to get fiducial parameter values for the SS simulations. The comparison between GWI and GWII gives out the model effect is small. The comparison between GWII and GWIII shows the friction term will shift the values of model parameters, especially Ω_{m0} .

1 Introduction

The standard siren (SS) provides an absolute measurement of distance without dependence on other sources [1]. This gravitational wave (GW) method is widely used to constrain cosmological models especially for the modified gravities. Presently, the direct detection of gravitational wave has discovered at least 99 GW events [2–8], but only one single confirmed standard siren event (GW170817) and one possible standard siren event (GW109521) detected. These two events are unable to do effective cosmological constraints. In the coming decade, ground-based (e.g. Einstein Telescope (ET) [9–11] and space-based GW (e.g. Taiji [12], Tianqin [13], and LISA [14]) experiments are predicted to discover more GW sources. Therefore, to forecast fundamental properties of gravities, the mock catalogs of standard sirens should be created.

The cosmological constant called Λ CDM model is the simplest theoretical explanation for the accelerating universe which is favored by Planck data [15, 16]. And, dark energy and modified gravities could make our universe accelerate as well. Obviously, the choice of fiducial model will affect the SS data simulation which is called model effect.

And compared with the Λ CDM and dark energy models, the propagation equation of gravitational wave modified gravity has an extra friction term which affects the SS simulation as well. It is called the extra friction term effect. Roughly, based on affine connections, there are mainly three types of modified gravity: $f(R)$, $f(T)$ and $f(Q)$ models [17–22]. Here, to see the differences between gravities, we choose the Λ CDM model in general relativity (GR) and the $f(Q)$ gravity which are relatively simple to discuss. Among the various $f(Q)$ models, the power exponential ($f(Q)|_{PE}$) model is chosen because it has been proved to alleviate the H_0 tension [23, 24]. And, it has the same free parameters with Λ CDM which could be regarded as a natural candidate of fiducial model in SS simulation. Meanwhile, under the constraining of EM data, the hyperbolic tangent ($f(Q)|_{HT}$) model is published by Akaike information criterion (AIC) and Bayesian information criterion (BIC) [25, 26] which worth further study. Therefore, the two $f(Q)$ models, which could not come back to Λ CDM models, are chosen to constrain.

Here, we intend to simulate three types of SS simulations: the first one (GWI) is based on the Λ CDM model; the second one (GWII) is based on the $f(Q)|_{PE}$ and $f(Q)|_{HT}$ models but assuming the extra friction term is zero; the third one (GWIII) is based on the two $f(Q)$ models as well but the extra friction term is non-zero. We will compare the GWI and GWII to see the model effect, and compare GWII and GWIII to see the effect of extra friction term. The electromagnetic (EM) data is used as standard including the type Ia supernovae (Pantheon), direct determination of the Hubble ($H(z)$), baryon acoustic oscillations (BAO), cosmic microwave background anisotropies (CMB) which all are related to the distance.

The rest of this paper is organized as follows. In Section 2, we will introduce the electromagnetic (EM) observational data and the simulated SS data employed in this work. In Section 3, we will briefly describe the two $f(Q)$

^ae-mail: zhangyia@cqupt.edu.cn

models used in this work. In Section 4, we will compare the SS data. In Section 5, we will report the constraint results. Finally, a brief summary will be given in Section 6.

2 The method

The Markov Chain Monte Carlo (MCMC) package CosmoMC [27] is employed to infer the posterior probability distributions of the cosmological parameters, and further to derive the best-fit values and corresponding errors. And numerical simulation is also used which presents as the valuable approach to forecast results of surveys and targeted observations. Furthermore, the Einstein Telescope, which will detect thousands of NSB (Neutron Star Binary) and BHB (Black Hole Binary) mergers to probe the cosmic expansion at high redshifts, is chosen as the representative of third generation instrument [28–30].

Firstly, we employ current EM observational data sets which are related to the cosmic distance, including the type Ia supernovae (Pantheon), the direct measurements of $H(z)$, the baryon acoustic oscillations (BAO) and the cosmic microwave background anisotropies (CMB), to perform the MCMC analysis and give out the fiducial parameter values required by SS simulation. The Pantheon compilation is comprised of 1048 SN data points at the redshift range of $0.01 < z < 2.26$ [31]. The distance modulus, which is the observable quantity in the supernovae(SN) data, is defined as

$$\mu = m - M = 5 \log_{10}[d_L(z)] + 5 \log_{10}\left[\frac{c/H_0}{\text{Mpc}}\right] + 25, \quad (1)$$

where

$$d_L = (1+z) \int_0^z \frac{d\tilde{z}}{H(\tilde{z})} \quad (2)$$

is the luminosity distance and $H_0 = 67.4 \text{ km/s/Mpc}$.

For the direct measurements of $H(z)$ that are related to the Hubble distance $D_H = c/H$, there are 41 data points [32–46]. The $H(z)$ data points can be obtained through two methods. One is based on cosmic chronometer which calculate the differential ages of passively evolving galaxies. The other one is based on the detection of radiation BAO features. The property of BAO in the clustering of matter in late universe could serve as a standard ruler to map the expansion history of the universe. In the BAO data, we use six measurements of the ratios of angular diameter distances and the so-called dilation scale $D_V(z) = (d_A^2(z)z/H(z))^{1/3}$ at various redshifts z from Refs. [47–49] where d_A is the angular distance.¹

Furthermore, the signal parameter R , involving the distance information in CMB, is defined as

$$R = \Omega_{m0}^{1/2} \int_0^{z_*} dz' / E(z'), \quad (3)$$

¹The measurement values of $H(z)$ and BAO are summarized in Ref. [50].

where $z_* = 1090.43$ denotes the decoupling redshift. In this work, we use the first year data from Planck mission which shows $R = 1.7499 \pm 0.0088$ [16].

The goodness of fit for the theoretical model is measured by the χ^2 and likelihood functions which are expressed as $\chi^2 = -2 \ln L$. The MCMC approach needs to minimize the value of χ^2 . Take the Pantheon data as example, it is

$$\chi_{\text{Pantheon}}^2 = \sum_{i=1}^{1048} \frac{\mu^{\text{theory}} - \mu^{\text{obs}}}{\sigma_{z_i}^2}, \quad (4)$$

where μ^{theory} and μ^{obs} indicate the theoretical and observed values of the distance modulus at redshift z_i respectively. The term $\sigma_{z_i}^2$ denotes the standard deviation associated with μ^{obs} . Likewise, we could write down the χ^2 of $H(z)$, BAO and CMB constraints. Then, we simulate the SS data by using the best-fit parameter values from EM data combination and the ET design index.

In modified gravities, the propagation equation of GW in Fourier form is [28, 30, 51]

$$\bar{h}_A'' + 2\mathcal{H}[1 + \delta(\eta)]\bar{h}_A' + k^2\bar{h}_A = 0, \quad (5)$$

where \bar{h}_A denotes the Fourier mode of the GW amplitude, $A = +, \times$ represent the polarizations, the prime “ \prime ” denotes a derivative with respect to conformal time η , and $\mathcal{H} = a'/a$. And especially, δ is the so-called extra friction term which is zero for the Λ CDM model or dark energy in GR.

The strain $h(t)$ in the GW interferometers could be written as [29]

$$h(t) = F_+(\theta, \phi, \psi)h_+(t) + F_\times(\theta, \phi, \psi)h_\times(t), \quad (6)$$

where F_+, F_\times are the antenna pattern functions sensed by the GW detector. The redshift range is chosen as $0 < z < 5$. And the GW sources considered in this work include the merger events from black hole-neutron star (BHNS) systems and binary neutron star (BNS) systems, both of which are expected to exhibit afterglows in the EM radiation after they emit bursts of GW. Thus, BNS and BHNS could be observed not only as a transient GW event, but also as an EM counterpart, and could be used as SS candidates.

In this work, we utilize the one-sided noise power spectral density (PSD) which characterize performance of the GW detector, to calculate the errors of the simulated data. The measurement errors of luminosity distance is also related to the weak lensing effects. Following the studies in Refs. [29, 52], this error is assumed to be $0.05z$. Thus, the total uncertainty on the measurement of D_L is taken as

$$\sigma_{D_L} = \sqrt{\sigma_{\text{inst}}^2 + \sigma_{\text{lens}}^2} = \sqrt{\left(\frac{2D_L}{\rho}\right)^2 + (0.05zD_L)^2}, \quad (7)$$

where σ_{inst}^2 is the instrumental error calculated by Fisher Matrix and ρ is the ratio of signal to noise which is usually chosen as $\rho > 8$. And likewise, we could give out the χ^2 of

the SS data as Eq.(4) as well. Then, the standard sirens observation offers a new independent way to probe the cosmic expansion.

In order to simplify the propagation equation within modified gravity theories, by defining a modified scale factor $\tilde{a}'/\tilde{a} = \mathcal{H}[1 + \delta(z)]$ and $\chi_A = \tilde{a}h_A$, we get [53]

$$\chi_A'' + \left(k^2 - \frac{\tilde{a}''}{\tilde{a}}\right) \chi_A = 0. \quad (8)$$

Then, the relation between the EM luminosity distance and the GW luminosity distance could be expressed as

$$D_L^{GW}(z) = \exp\left(\int_0^z \frac{\delta(z')}{1+z'} dz'\right) D_L^{EM}(z), \quad (9)$$

where $D_L^{EM}(z)$ is EM luminosity distance. Obviously, the extra friction term δ characterizes the difference between the GW luminosity distance and the EM luminosity distance. When δ is negative, $D_L^{EM} > D_L^{GW}$, there is a smaller D_L^{GW} which denotes a larger H , and then a larger H_0 . The H_0 parameter is related with the famous Hubble tension where the Hubble constant H_0 inferred from the Planck CMB observation combined with the Λ CDM model [15] is about 5σ tension with the direct measurements by the SH0ES (Supernovae H0 for the Equation of State) team [54]. Many models which could return to the Λ CDM meet H_0 tension problem as the Λ CDM model does [55, 56]. So, we choose the Λ CDM model and two non-typical $f(Q)$ models to make comparisons. The calculated values of H_0 tension from different data combinations could be denoted as [57]

$$T_1(\theta) = \frac{|\theta(D_1) - \theta(D_2)|}{\sqrt{\sigma_\theta^2(D_1) + \sigma_\theta^2(D_2)}}. \quad (10)$$

Here, θ is chosen as the best-fitted values of H_0 from different data sets; the first data set D_1 represents the data combinations used in cosmological fitting; the second data set D_2 represents the $H_0 = 73.04 \pm 1.04 \text{ km} \cdot \text{s}^{-1} \cdot \text{Mpc}^{-1}$ from the SH0ES Team [54]; $\sigma_\theta(D_1)$ and $\sigma_\theta(D_2)$ represent the absolute errors from D_1 and D_2 data sets, respectively.

In this paper, we will simulate 1000 standard siren data points expected to be detected by ET in its 10-year observation. To achieve this, the Fisher matrix approach is utilized [30]. And, we roughly assume that there are 500 BNS events and 500 BHNS events.

3 The $f(Q)$ cosmology

In the Symmetric Teleparallel gravity, the non-metricity Q , which represents the variation in the length of a vector during parallel transport, is used to describe the gravitational interaction. And, its natural extension, the $f(Q)$ modified gravity, has revealed many interesting cosmological phenomena as shown in the literature [23, 24, 58–88].²

²The description of gravity using Teleparallel Gravity with Weitaenböck connection T which is called torsion scalar as well

The action of $f(Q)$ cosmology could be given by [58–60],

$$S = \int \sqrt{-g} \left[-\frac{1}{16\pi G} f(Q) + \mathcal{L}_m \right] d^4x, \quad (11)$$

where $f(Q)$ is an arbitrary function of the non-metricity scalar Q ; \mathcal{L}_m is the matter Lagrangian density and g is the determinant of the metric $g_{\mu\nu}$.

As the flat, homogeneous and isotropic Friedmann-Robertson-Walker (FRW) spacetime is considered, we obtain the non-metricity scalar as

$$Q = 6H^2. \quad (12)$$

Here, $H = \dot{a}/a$ is the Hubble parameter. Note that in the $f(Q)$ gravity theories, the non-metricity scalar Q plays the role of Ricci scalar R in GR, which indicates these two categories of modified gravity theories ($f(Q)$ and $f(R)$) are equivalent in the background level. It is convenient to set $f(Q) = Q + F(Q)$ where the $F(Q)$ part represents the cosmic acceleration effect. And under the above conditions, the Friedmann equations take the form [58–60]

$$3H^2 = \rho + \frac{F}{2} - QF_Q, \quad (13)$$

$$\dot{H} = \frac{F - Q - 2QF_Q}{4(2QF_{QQ} + F_Q + 1)}, \quad (14)$$

where ρ and p are the energy density and pressure for the matter fluid, and satisfy the conservation equation:

$$\dot{\rho} + 3H(1+w)\rho = 0, \quad (15)$$

where w is the equation-of-state (EoS) parameter.

Correspondingly, the effective energy density ρ_{eff} and effective pressure p_{eff} for the acceleration part that is sourced from $F(Q)$ could be described as

$$\rho_{\text{eff}} = \frac{F}{2} - QF_Q, \quad (16)$$

$$p_{\text{eff}} = 2\dot{H}(2QF_{QQ} + F_Q) - \rho_{\text{eff}}. \quad (17)$$

Thus, the effective EoS parameter could be given by

$$w_{\text{eff}} = -1 + \frac{1 - 1/(F/Q - 2F_Q)}{1 + 1/(2QF_{QQ} + F_Q)}. \quad (18)$$

In the framework of $f(Q)$ gravity, the extra friction term δ takes the form

$$\delta(z) = \frac{d \ln f_Q}{2\mathcal{H} d\eta}. \quad (19)$$

And the dimensionless Hubble parameter could be expressed as

$$E(z) = \frac{H}{H_0}, \quad (20)$$

where the subscript “0” denotes the present time.

is equivalent with the Symmetric Teleparallel gravity using the non-metricity scalar Q in the background level where the curvature R in GR is replaced by T or Q [50, 89–106].

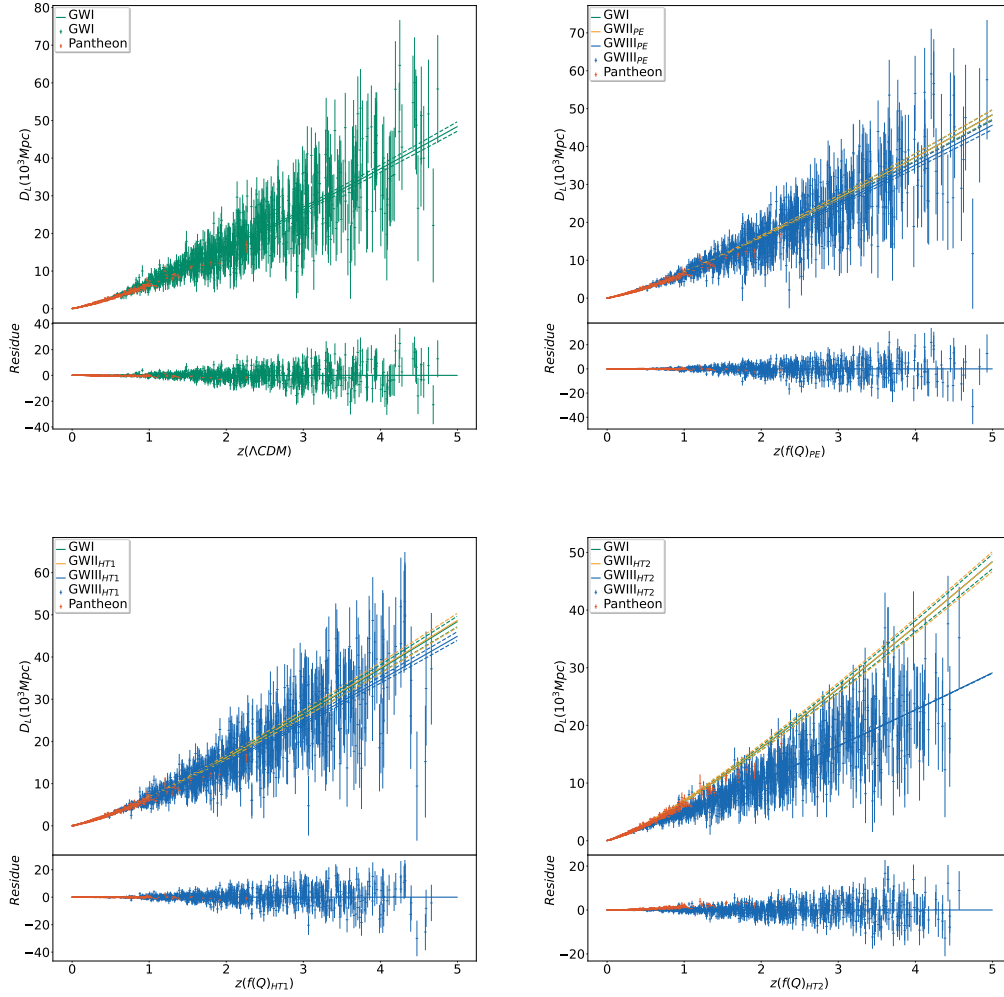


Fig. 1 The red one with error-bar are the real data: Pantheon combination. The green one with error-bar are GWI data which based on Λ CDM model with $\Omega_{m0} = 0.287$ and $H_0 = 70.10$. The blue one with error-bar are GWIII data which based on $f(Q)$ models with different best fitted values. The lines denote the evolutions of D_L by assuming the initial values as the best fitted values (solid) and the 1σ errors (dashed) from the EM fitting results separately.

3.1 The Power Exponential form: $f(Q)_{PE}$ model

In Refs. [23, 24], a power exponential form of $f(Q)$ model has been introduced (hereafter $f(Q)_{PE}$ model for convenience), and it could be expressed as:

$$F(Q) = Q \left(e^{\lambda \frac{Q_0}{Q}} - 1 \right), \quad (21)$$

where the derived parameter λ which is determined by Ω_{m0} could be described as

$$\lambda = \frac{1}{2} + W_0 \left(-\frac{\Omega_{m0}}{2e^{\frac{1}{2}}} \right). \quad (22)$$

And, W_0 is the Lambert function. Similar to the Λ CDM model, the $f(Q)_{PE}$ model has two free parameters Ω_{m0} and H_0 roughly. Note that, the $f(Q)_{PE}$ model theoretically could not come back to the Λ CDM for any values of λ , thus is called the non-typical model here.

At high-redshift range where $Q_0 \ll Q$, we can get $F_Q \simeq -\lambda^2 Q_0^2 / Q^2$ and $F_{QQ} \simeq \lambda^2 Q_0^2 / Q^3$ which are small. When $Q_0 \ll Q$, the effective EoS can be expanded as

$$w_{\text{eff}} = -1 - \lambda \frac{Q_0}{Q}. \quad (23)$$

If $\lambda > 0$, the w_{eff} would approach to -1 from the phantom side. The extra friction term could be expressed as

$$\delta = -\frac{3}{2} \lambda^2 \left(\frac{Q_0}{Q} \right)^2, \quad (24)$$

which is tend to 0 from negative side.

According to Eq.(9), the luminosity distance will change with $\delta \neq 0$. To investigate the impacts of δ , we simulate the SS data based on $\delta = 0$ (GWII_{PE}) and $\delta \neq 0$ (GWIII_{PE}).

Table 1 Best fitted values with 1σ and 2σ standard errors from the constraints of EM, GWI, GWII and GWIII data on the Λ CDM, $f(Q)_{PE}$, $f(Q)_{HT1}$ and $f(Q)_{HT2}$ models.

Model	Data	Ω_{m0}	H_0 (km/s/Mpc)	n	δ_0	$w_{\text{eff}0}$	H_0 Tension	χ^2
Λ CDM	EM	$0.290^{+0.010+0.019}_{-0.010-0.019}$	$68.20^{+1.00+2.00}_{-1.00-2.00}$	—	0	—1	3.35σ	1063.4
	GWI	$0.298^{+0.012+0.025}_{-0.012-0.024}$	$67.83^{+0.43+0.84}_{-0.43-0.84}$	—	0	—1	4.63σ	981.6
$f(Q)_{PE}$	EM	$0.287^{+0.010+0.020}_{-0.010-0.019}$	$70.10^{+1.10+2.20}_{-1.10-2.10}$	—	$-0.085^{+0.001+0.003}_{-0.001-0.003}$	$-1.111^{+0.004+0.007}_{-0.004-0.007}$	1.94σ	1075.5
	GWI	$0.322^{+0.012+0.024}_{-0.012-0.023}$	$68.56^{+0.43+0.83}_{-0.43-0.84}$	—	$-0.090^{+0.001+0.002}_{-0.001-0.002}$	$-1.124^{+0.004+0.008}_{-0.004-0.008}$	3.98σ	983.4
	GWII _{PE}	$0.312^{+0.016+0.032}_{-0.016-0.029}$	$69.51^{+0.66+1.31}_{-0.66-1.31}$	—	$-0.089^{+0.002+0.003}_{-0.002-0.003}$	$-1.120^{+0.006+0.011}_{-0.006-0.011}$	2.87σ	985.6
	GWIII _{PE}	$0.331^{+0.014+0.031}_{-0.016-0.029}$	$71.59^{+0.64+1.20}_{-0.64-1.20}$	—	$-0.090^{+0.001+0.003}_{-0.001-0.003}$	$-1.127^{+0.005+0.010}_{-0.005-0.011}$	1.19σ	982.5
$f(Q)_{HT1}$	EM	$0.292^{+0.010+0.020}_{-0.010-0.020}$	$68.60^{+1.20+2.40}_{-1.20-2.30}$	$0.186^{+0.081+0.140}_{-0.061-0.150}$	$0.031^{+0.033+0.081}_{-0.045-0.076}$	$-0.869^{+0.052+0.140}_{-0.076-0.120}$	2.80σ	1065.1
	GWI	$0.333^{+0.017+0.034}_{-0.017-0.032}$	$67.26^{+1.11+1.91}_{-0.82-2.10}$	$0.040^{+0.331+0.460}_{-0.151-0.520}$	$0.001^{+0.063+0.250}_{-0.131-0.201}$	$-0.905^{+0.101+0.431}_{-0.231-0.340}$	4.08σ	981.7
	GWII _{HT1}	$0.321^{+0.017+0.035}_{-0.017-0.033}$	$67.38^{+2.01+3.20}_{-1.60-3.51}$	$0.050^{+0.330+0.450}_{-0.151-0.651}$	$0.029^{+0.074+0.351}_{-0.190-0.251}$	$-0.856^{+0.110+0.620}_{-0.320-0.410}$	2.74σ	985.0
	GWIII _{HT1}	$0.388^{+0.017+0.035}_{-0.017-0.033}$	$67.42^{+0.93+1.80}_{-0.93-1.70}$	$0.299^{+0.171+0.205}_{-0.039-0.302}$	$0.156^{+0.111+0.290}_{-0.181-0.242}$	$-0.600^{+0.201+0.580}_{-0.351-0.452}$	4.03σ	978.2
$f(Q)_{HT2}$	EM	$0.294^{+0.010+0.021}_{-0.010-0.020}$	$68.48^{+1.20+2.51}_{-1.20-2.41}$	$1.603^{+0.021+0.041}_{-0.021-0.043}$	$-0.459^{+0.041+0.071}_{-0.031-0.075}$	$-1.006^{+0.018+0.036}_{-0.018-0.035}$	2.87σ	1069.4
	GWI	$0.263^{+0.057+0.084}_{-0.047-0.085}$	$67.51^{+0.55+1.10}_{-0.55-1.00}$	$1.740^{+0.170+0.206}_{-0.086-0.240}$	$-0.280^{+0.190+0.241}_{-0.110-0.260}$	$-0.880^{+0.141+0.180}_{-0.099-0.190}$	4.70σ	980.9
	GWII _{HT2}	$0.279^{+0.052+0.067}_{-0.023-0.093}$	$68.17^{+0.68+1.20}_{-0.59-1.30}$	$1.653^{+0.040+0.234}_{-0.153-0.153}$	$-0.404^{+0.099+0.291}_{-0.211-0.252}$	$-0.964^{+0.041+0.201}_{-0.131-0.141}$	4.00σ	979.0
	GWIII _{HT2}	$0.449^{+0.001+0.001}_{-0.001-0.002}$	$74.84^{+0.22+0.42}_{-0.22-0.42}$	$1.945^{+0.001+0.001}_{-0.001-0.002}$	$-0.026^{+0.001+0.002}_{-0.001-0.002}$	$-0.450^{+0.001+0.002}_{-0.001-0.003}$	1.69σ	1607.7

3.2 The Hyperbolic Tangent form: $f(Q)_{HT}$ model

For the purpose of realizing the crossing of the phantom divide line for the effective equation of state [107], the hyperbolic tangent form of the $f(Q)$ model is proposed as [50, 108] (hereafter $f(Q)_{HT}$ model):

$$F(Q) = \alpha Q_0 \left(\frac{Q_0}{Q} \right)^{-n} \tanh \frac{Q_0}{Q}, \quad (25)$$

where n is an additional free parameter compared with Λ CDM model or $f(Q)_{PE}$ model. And the dimensionless parameter α could be expressed as

$$\alpha = \frac{1 - \Omega_{m0}}{(1 - 2n) \tanh 1 + 2 \operatorname{sech}^2 1}. \quad (26)$$

The $f(Q)_{HT}$ model could not come back to the Λ CDM for any values of n as well.

When $Q \gg Q_0$, $\tanh(Q_0/Q) \simeq Q_0/Q$ and $\operatorname{sech}(Q_0/Q) \simeq 1$. Then, $F_Q \simeq \alpha(n-1)(Q_0/Q)^{(2-n)}$ and $F_{QQ} \simeq \alpha(1-n)(2-n)(Q_0/Q)^{(2-n)}/Q$ which are small as well at high redshift. And, the EoS and δ is approximately to be

$$w_{\text{eff}} = -2 + n, \quad (27)$$

$$\delta = -\alpha(1-n)(2-n) \left(\frac{Q_0}{Q} \right)^{2-n}. \quad (28)$$

As the effective energy density must be larger than 0, we need to give a prior of n for the model. So, we divide the Hyperbolic Tangent model to two branches:

$f(Q)_{HT1}$: $n < 0.5$. The w_{eff} would approach to the phantom side at high redshifts. The δ tends to 0 from negative side.

$f(Q)_{HT2}$: As BBN give the constraint $n < 1.946$ [109]³, we set a prior $1.500 < n < 1.946$. So, the w_{eff} would approach to the quintessence side at high redshifts. The δ tends to 0 from positive side.

4 The Simulated SS data

Here, we summary the used data as below:

EM: The Pantheon+H(z)+BAO+CMB observational combination which has 1096 data is standard whose best fitted values are used as initial parameter values in SS simulations. We list the constraining results in Table 1.

GWI: The GWI simulation is based on the Λ CDM model with $\Omega_{m0} = 0.287$ and $H_0 = 70.10$. This simulation is mainly used for comparison [24].

GWII: As Table 1 shows, we use $f(Q)_{PE}$ model with $\Omega_{m0} = 0.287$ and $H_0 = 70.10$ for the GWII simulation; $f(Q)_{HT1}$ model with $\Omega_{m0} = 0.292$, $H_0 = 68.60$ and $n = 0.186$ for the GWII_{HT1} simulation; and $f(Q)_{HT2}$ model with $\Omega_{m0} = 0.294$, $H_0 = 68.48$ and $n = 1.603$ for the GWIII_{HT2} simulation. Especially, $\delta = 0$ is assumed for all the GWII

³Another BBN constraints for the $f(Q)_{HT2}$ model are satisfied $n \lesssim 1.88$ [108].

simulations for comparison. Physically, the GWII simulations do not correspond to any true data.

GWIII: The model parameter values are the same as GWII except that we use $\delta_0 = -0.085$, $\delta_0 = 0.031$ and $\delta_0 = -0.459$ which are the EM constraining results listed in Table 1 for the GWIII_{PE} , GWIII_{HT1} and GWIII_{HT2} separately.

4.1 The D_L data comparison

We list the luminosity distance (D_L) data in Fig. 1, including the Pantheon, the simulated GWI and GWIII data. And for comparison, we plot the evolution lines of D_L based on the different fiducial models.

As the residues show, the simulated data consist with their fiducial models and parameter values. The evolution lines based on GWI and GWII are closed to each other for all the models. And the GWII related regimes are slightly narrower. This indicates that the constraining results of GWI and GWII will be similar. And for the $f(Q)_{EP}$ and $f(Q)_{HT1}$ models, the simulated data GWIII have larger D_L values when $z > 1.8$ which will make a large Ω_{m0} compared with the real data (Pantheon). For the $f(Q)_{HT2}$ model, the situation is opposite where the simulated data GWIII have smaller values when $z > 1$.

4.2 The criterion

The χ^2 s of simulated SS data list in Table 2 are around 1000 which could be regarded as reasonable. For comparison, we list the constraining results of Λ CDM model as well. Furthermore, we will make a comparison for the EM and GWI results by using the Akaike information criteria (AIC) where $AIC = \chi^2 + 2n$ with n is the number of free parameter [110] and the Bayesian information criteria (BIC) where $BIC = \chi^2 + n \ln m$ with m is the number of data points used in the fit [111]. For Gaussian errors, the difference between two models could be written as $\Delta AIC = \Delta \chi^2 + 2\Delta n$. Similar to the AIC, the difference denoted by BIC has the form $\Delta BIC = \Delta \chi^2 + \Delta n \ln m$. The $\Delta AIC = 5/\Delta BIC \geq 2$ and $\Delta AIC = 10/\Delta BIC \geq 6$ are considered to be the positive and strong evidence against the weaker model.

5 Results and discussion

The constraining best fitted parameter values with 1σ and 2σ standard errors are listed in Table 1. Correspondingly, the triangle plots, including the probability density function (pdf) and the contours for the model parameters in Λ CDM, $f(Q)_{PE}$, $f(Q)_{HT1}$ and $f(Q)_{HT2}$ models are presented in Figs. 2, 3, 5 and 7 respectively. Generally, the contours are closed

and smooth. And the pdfs are Gaussian-distributed for all the models except the GWIII results of $f(Q)_{HT2}$ model. In Fig. 2, the $\Omega_{m0} - H_0$ contour of GWI shows a smaller regime of H_0 compared to the EM result in Λ CDM model. Similar to Λ CDM model, the results of SS data have tighter constraining ability than that of EM data in the $f(Q)_{PE}$ model. Oppositely, the results of EM data have tighter constraining ability than that of SS data in the $f(Q)_{HT1}$ model. Especially, all the physical SS related H_0 s are tighter than the ones from EM. Roughly speaking, the SS data has comparable ability with the EM data on constraining model parameters.

As predicted by Fig. 1, the results derived from EM, GWI and GWII are close to each other for all models. And, the results of GWII and GWIII with the similar shapes have larger parameter ranges than that GWI. The phenomenon denotes the model effect is small but should not be ignored. And, the constrained parameters derived from GWIII (especially Ω_{m0}) show a large shift compared with that from GWII. This phenomenon denotes the addition friction term δ plays an important effect for the modified gravities.

As supplements, we list the χ^2 results in Table 2. And we also plot the 1σ evolutions of δ and w_{eff} in Figs. 4, 6 and 8 for $f(Q)_{PE}$, $f(Q)_{HT1}$ and $f(Q)_{HT2}$ models.

5.1 The $f(Q)_{PE}$ model

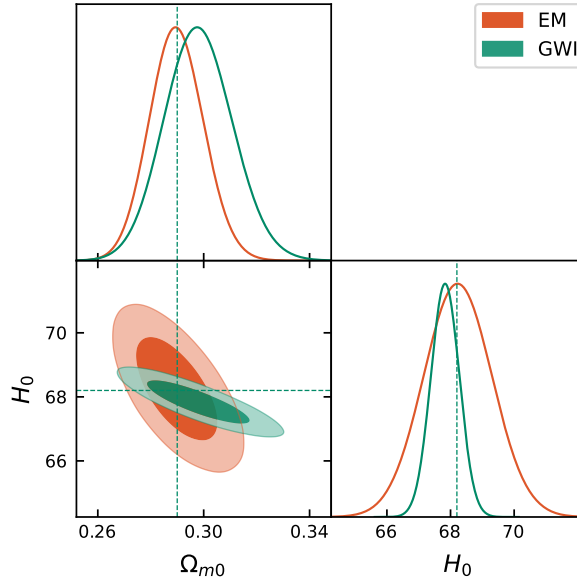
As Table 1 and Fig. 3 show, the parameter δ_0 is always smaller than 0, which means that the luminosity distances of SS data (D_L^{GW}) are smaller than that of EM data according to Eq. (9). The best fitted values and their 2σ regimes of δ are around -0.085 from all the data. Precisely speaking, the $\delta_0 = 0$ is excluded in all the results of the $f(Q)_{PE}$ model. That makes a larger Ω_{m0} . The phenomenon denotes that the derived parameter δ shifts the model parameters and affects the constraining precision slightly. And when $z = 0$, $Q = Q_0$, as Eq.(9) shown, the δ_0 and $w_{\text{eff}0}$ are mainly determined by the dimensionless parameter Ω_{m0} in this model. Then it is not a surprise that the shapes of contours $\delta_0 - w_{\text{eff}0}$ are narrow and similar for all the models. And as Eq.(24) and Fig. 4 show at high z , δ tend to 0 which corresponding to Λ CDM model.

All the constraint results exclude $w_{\text{eff}} = -1$ in 2σ regimes which means this model could be distinguished from the Λ CDM model. In Fig. 4, with increasing of redshift z , the evolving shape of w_{eff} and δ are similar which corresponds to the narrow positive correlation of w_{eff} and δ in Fig. 3. The value of w_{eff} gradually approaches -1 , which mimics the standard Λ CDM model but still phantom.

Compared with Λ CDM model shown in Fig. 2, the H_0 related contours derived from the SS data are parallel. As shown in Table 1, the H_0 tension could be alleviated with the price of increasing Ω_{m0} . Particularly, the H_0 tension could be relieved to 1.19σ level under the constraint of GWIII. The

Table 2 The calculated values of χ^2 , AIC and BIC for the Pantheon, $H(z)$, BAO, CMB, EM and GWI data.

Model	$\chi^2_{Pantheon}$	$\chi^2_{H(z)}$	χ^2_{BAO}	χ^2_{CMB}	AIC_{EM}	BIC_{EM}	ΔAIC_{EM}	ΔBIC_{EM}	AIC_{GWI}	BIC_{GWI}	ΔAIC_{GWI}	ΔBIC_{GWI}
Λ CDM	1036.4	23.3	3.2	0.5	1067.4	1077.4	0	0	985.6	995.4	0	0
$f(Q)_{PE}$	1045.8	25.4	2.6	1.7	1079.5	1089.5	12.1	12.1	987.4	997.2	1.8	1.8
$f(Q)_{HT1}$	1038.1	22.7	3.4	0.9	1071.1	1086.1	3.7	8.7	987.7	1002.4	2.1	7.0
$f(Q)_{HT2}$	1038.6	27.0	2.7	1.1	1075.4	1090.4	8.0	13.0	986.9	1001.6	1.3	6.2

**Fig. 2** The probability density functions, 1σ and 2σ confidence regions for the parameters (Ω_{m0} and H_0) in the Λ CDM model. The dashed lines denote the best fitted values of EM data.

$f(Q)_{PE}$ model are consistent with the observation from the SH0ES Team.

In the $f(Q)_{PE}$ model, the $\Delta AIC_{EM} = \Delta BIC_{EM} = 12.1$ which is caused by the Pantheon data mainly and punished by the information criterion. Anyway, the large χ^2 from Pantheon is still smaller than the data number. And the SS data give out low ΔAIC and ΔBIC for the $f(Q)_{PE}$ model.

5.2 The $f(Q)_{HT1}$ model

As shown in Table 1, the constraint of $f(Q)_{HT1}$ model from the EM data has similar values of Ω_{m0} and H_0 with the case of Λ CDM. But $w_{\text{eff}} = -1$ is excluded in 2σ confidence interval in the EM results.

As Fig. 1 shows, the D_L of GW is smaller than that of EM. Correspondingly, the results from the SS data favors a much larger Ω_{m0} compared with the results from EM data. In the constraint results of GWIII data, the best fitted result of Ω_{m0} reaches 0.388. And, the $\delta_0 = 0$ and $w_{\text{eff}} = -1$ are

included in all the GW related results. There is a tension between the EM and all the SS data.

The $f(Q)_{HT1}$ model has one more free parameter n than the $f(Q)_{PE}$ model which make the δ cross 0 and w_{eff} cross -1 in most results as Fig. 6 shows. And with the increasing of z , δ s gradually approach 0, w_{eff} s deviate from -1 and gradually approach -2 .

And, in the $f(Q)_{HT1}$ model, $\Delta AIC_{EM} = 3.7$ and $\Delta AIC_{GWI} = 2.1$ which is favored, but $\Delta BIC_{EM} = 8.7$ and $\Delta BIC_{GWI} = 7.0$ which is punished by the BIC.

5.2.1 The $f(Q)_{HT2}$ model

Because the fiducial model has a rather large negative δ_0 which is -0.459 , D_L of GWIII simulation is much smaller than that of EM data and other simulations as Fig. 1 shows. As a consequence, the GWIII could not give out an effective Ω_{m0} even after set a prior $0 < \Omega_{m0} < 0.45$ as Table 1 and Fig. 7 show. Then, the constraining results of GWIII where $\Omega_{m0} = 0.449^{+0.001+0.001}_{-0.001-0.002}$ could not give out an effective constraint. And as Fig. 8 shows, this constraining results favor

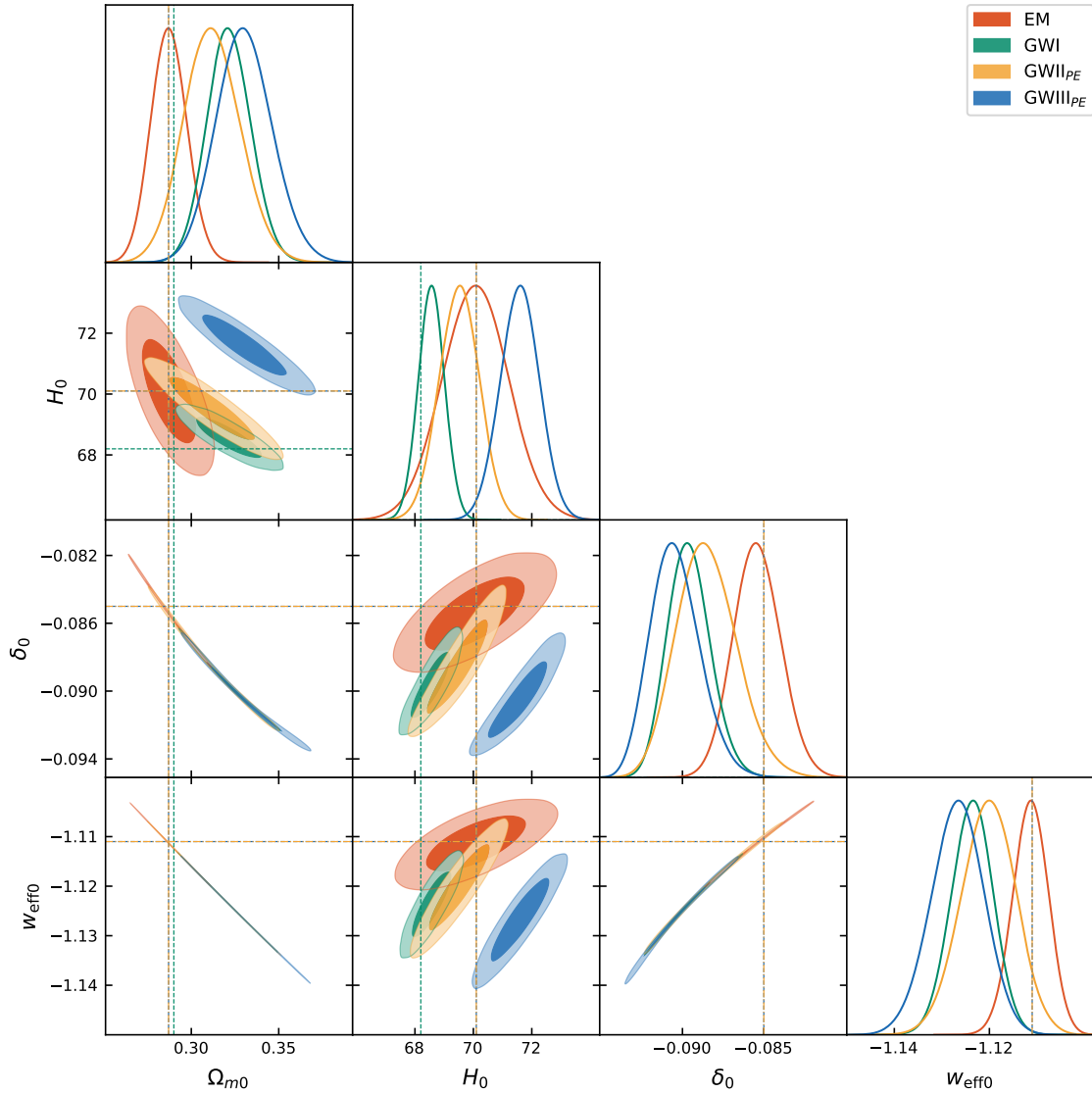


Fig. 3 The probability density functions, 1σ and 2σ confidence regions for the parameters (Ω_{m0} , H_0 , δ_0 and $w_{\text{eff}0}$) in the $f(Q)_{PE}$ model. The dashed lines denote the best fitted values. The green dashed lines denote the best fitted values of EM data for Λ CDM model which we used to simulate GWI data. The orange dashed lines and the blue dotted denote the best fitted values of EM data of $f(Q)_{PE}$ model which we used to simulate GWII and GWIII data.

a matter dominated universe ($w_{\text{eff}} \sim -0.055$) at about $z \sim 2$. Though the other data give reasonable results, we still conclude that the $f(Q)_{HT}$ model could be ruled out by the future GW observational data because of such poor fitting results where $\chi^2 = 1067.7$ of GWIII. As the $f(Q)_{HT2}$ model is excluded, it is no need to discuss its *AIC* and *BIC* exactly.

6 Conclusion

As the effects that affect the GW simulation are mainly the model and the extra friction term, we simulated SS data based on Λ CDM (GWI), the $f(Q)$ models with $\delta = 0$ (GWII) and the $f(Q)$ models with $\delta \neq 0$ (GWIII), and use the cur-

rent EM observational data as supplements. And the $f(Q)_{PE}$ and $f(Q)_{HT}$ models which could not come back to Λ CDM model are chosen to constrain.

The $f(Q)_{PE}$ model are consistent with SS data. Especially for the SS data, the Hubble tension could be alleviated, especially to be 1.19σ level with the GWIII_{PE} constraints. The SS data could distinguish the $f(Q)_{PE}$ model and Λ CDM model. For the EM data, The $f(Q)_{PE}$ model has large *AIC*.

The $f(Q)_{HT1}$ model, for the SS data, Ω_{m0} increased compared to the EM data. And the *AIC* increased which means the $f(Q)_{HT1}$ model is not favored by the SS data or the EM data. The constraining results of GWIII could not give out an

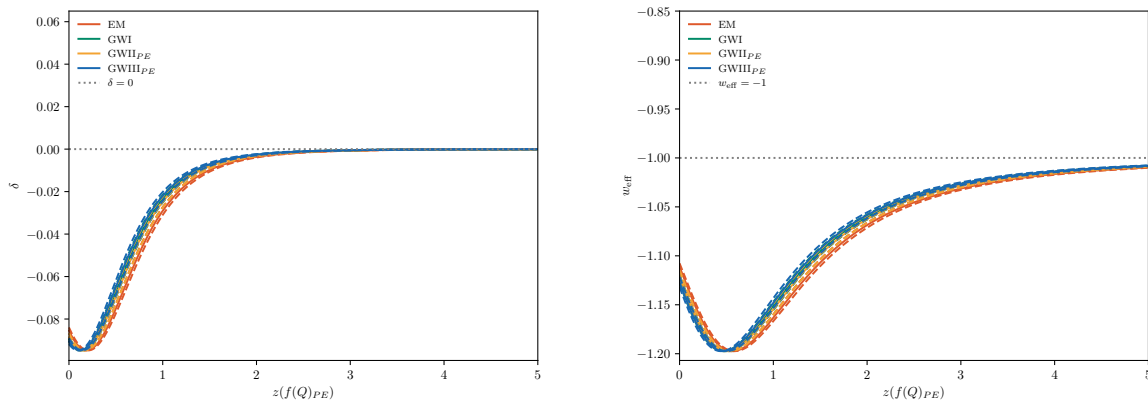


Fig. 4 The evolutions of δ and w_{eff} within 1σ confidence intervals for the $f(Q)_{PE}$ model under the constraints of EM, GWI, GWII and GWIII data. The solid lines denote the best fitted values. The dashed lines denote the 1σ regions. The dotted line denotes $w_{\text{eff}} = -1$ which is the Λ CDM model.

effective Ω_{m0} for $f(Q)_{HT2}$ model. Therefore, the $f(Q)_{HT2}$ model are excluded by the true SS data.

The constraining results from GWI and GWII are similar, the effect of the fiducial model is small. And the comparison between GWII and GWIII shows, the friction term brings large shift to parameters. In a conclusion, the SS data has the ability to break the model degenerations. And the notable effect of δ parameter should not be ignored.

7 Acknowledgements

YZ is supported by National Natural Science Foundation of China under Grant No.12275037 and 12275106. DZH is supported by the Talent Introduction Program of Chongqing University of Posts and Telecommunications (grant No. E012A2021209) the Youth Science and technology research project of Chongqing Education Committee (Grant No. KJQN202300609).

References

1. B.F. Schutz, *Nature* **323**, 310 (1986). DOI 10.1038/323310a0
2. B.P. Abbott, et al., *Phys. Rev. Lett.* **116**(6), 061102 (2016). DOI 10.1103/PhysRevLett.116.061102
3. B.P. Abbott, et al., *Phys. Rev. X* **6**(4), 041015 (2016). DOI 10.1103/PhysRevX.6.041015. [Erratum: *Phys.Rev.X* 8, 039903 (2018)]
4. B.P. Abbott, et al., *Nature* **551**(7678), 85 (2017). DOI 10.1038/nature24471
5. B.P. Abbott, et al., *Phys. Rev. Lett.* **118**(22), 221101 (2017). DOI 10.1103/PhysRevLett.118.221101. [Erratum: *Phys.Rev.Lett.* 121, 129901 (2018)]
6. B.P. Abbott, et al., *Phys. Rev. Lett.* **119**(14), 141101 (2017). DOI 10.1103/PhysRevLett.119.141101
7. R. Abbott, et al., *Phys. Rev. X* **11**, 021053 (2021). DOI 10.1103/PhysRevX.11.021053
8. R. Abbott, et al., *Astrophys. J. Lett.* **915**(1), L5 (2021). DOI 10.3847/2041-8213/ac082e
9. M. Punturo, et al., *Class. Quant. Grav.* **27**, 194002 (2010). DOI 10.1088/0264-9381/27/19/194002
10. B.S. Sathyaprakash, B.F. Schutz, C. Van Den Broeck, *Class. Quant. Grav.* **27**, 215006 (2010). DOI 10.1088/0264-9381/27/21/215006
11. X.N. Zhang, L.F. Wang, J.F. Zhang, X. Zhang, *Phys. Rev. D* **99**(6), 063510 (2019). DOI 10.1103/PhysRevD.99.063510
12. W.R. Hu, Y.L. Wu, *Natl. Sci. Rev.* **4**(5), 685 (2017). DOI 10.1093/nsr/nwx116
13. J. Luo, et al., *Class. Quant. Grav.* **33**(3), 035010 (2016). DOI 10.1088/0264-9381/33/3/035010
14. Laser interferometer space antenna: A cornerstone mission for the observation of gravitational waves. Tech. rep., NASA (2011). URL https://lisa.nasa.gov/archive2011/Documentation/sts_1.04.pdf
15. P.A.R. Ade, et al., *Astron. Astrophys.* **594**, A13 (2016). DOI 10.1051/0004-6361/201525830
16. P.A.R. Ade, et al., *Astron. Astrophys.* **571**, A16 (2014). DOI 10.1051/0004-6361/201321591
17. M. Braglia, M. Ballardini, F. Finelli, K. Koyama, *Phys. Rev. D* **103**(4), 043528 (2021). DOI 10.1103/PhysRevD.103.043528
18. P. Brax, C. van de Bruck, S. Clesse, A.C. Davis, G. Sculthorpe, *Phys. Rev. D* **89**(12), 123507 (2014). DOI 10.1103/PhysRevD.89.123507
19. T. Clifton, P.G. Ferreira, A. Padilla, C. Skordis, *Phys. Rept.* **513**, 1 (2012). DOI 10.1016/j.physrep.2012.01.001

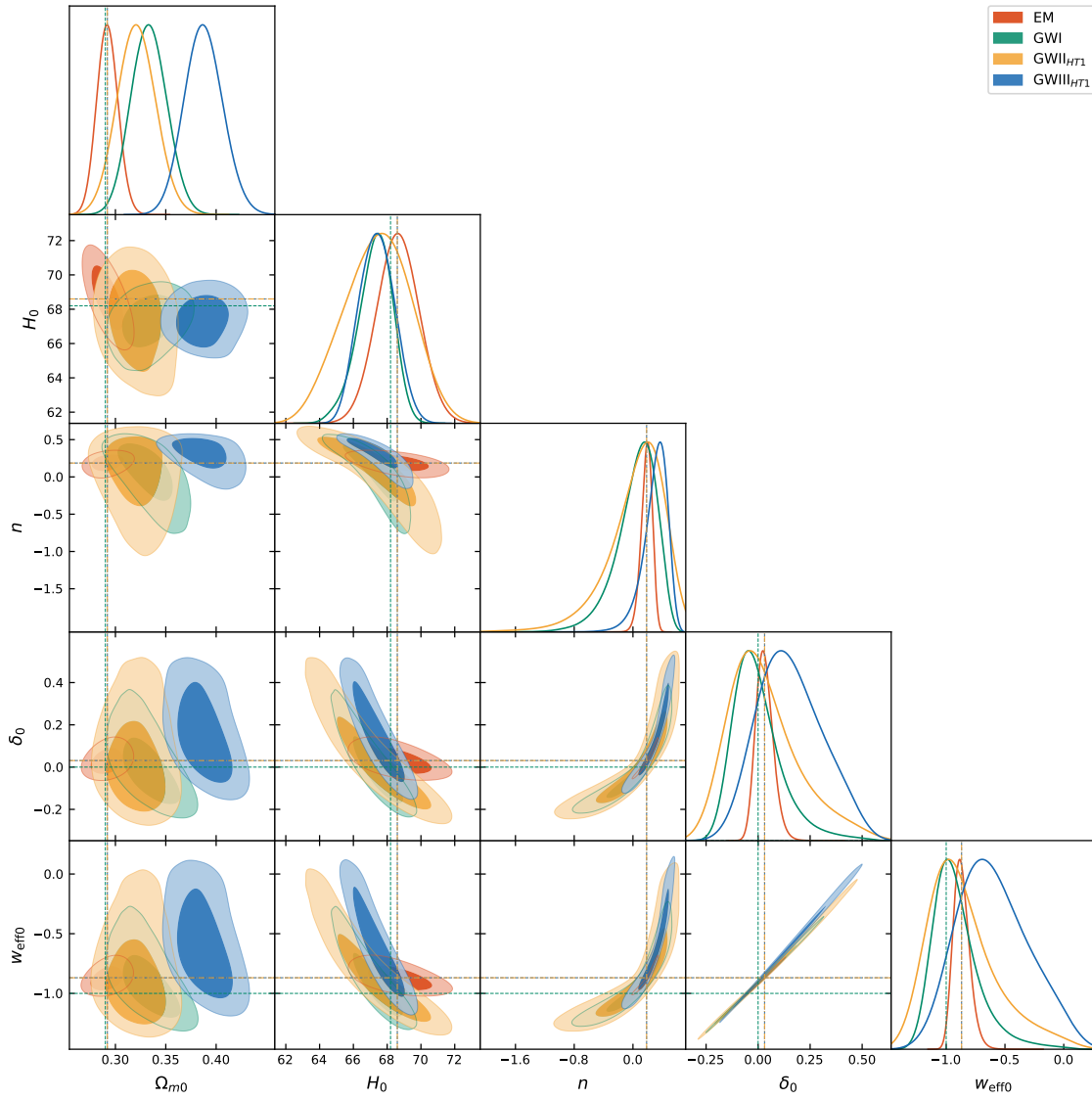


Fig. 5 The probability density functions, 1σ and 2σ confidence regions for the parameters Ω_{m0} , H_0 , n , δ_0 and $w_{\text{eff}0}$, respectively in the $f(Q)_{HT1}$ model. The others are the same as Fig. 3.

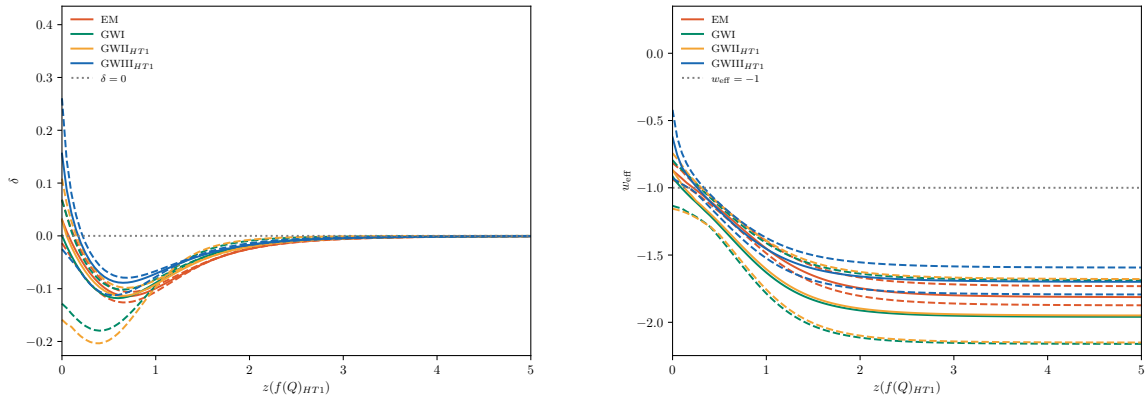


Fig. 6 Same as Fig. 4, but for the $f(Q)_{HT1}$ model.

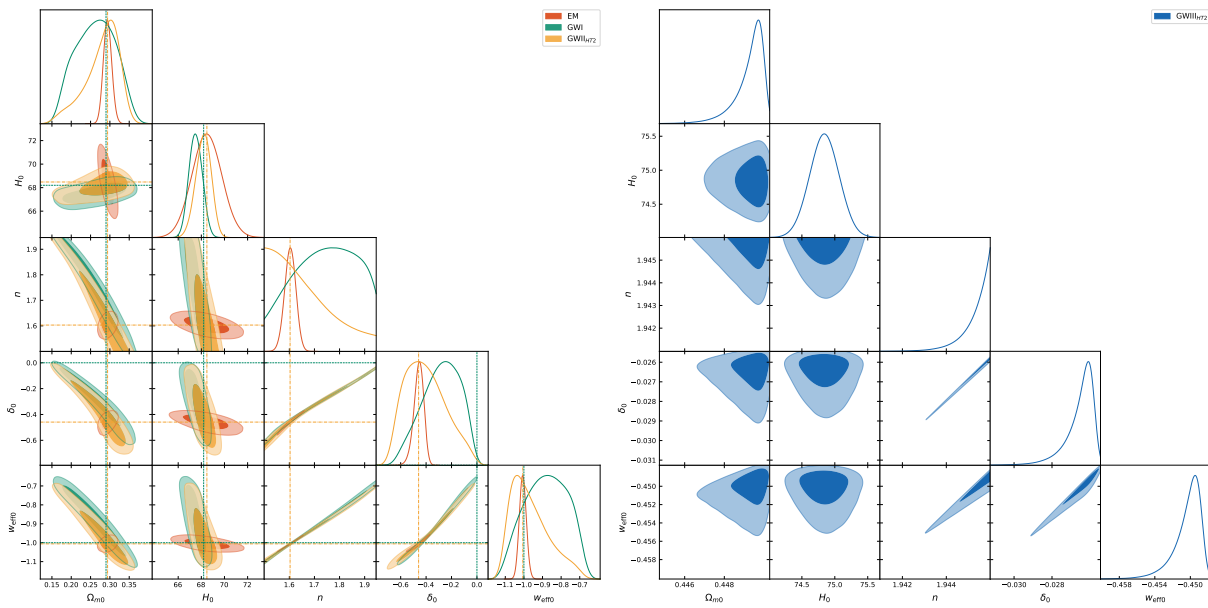


Fig. 7 Same as Fig. 5 but for the $f(Q)_{HT2}$ model, except the results of GWIII data are too small which we list separately.

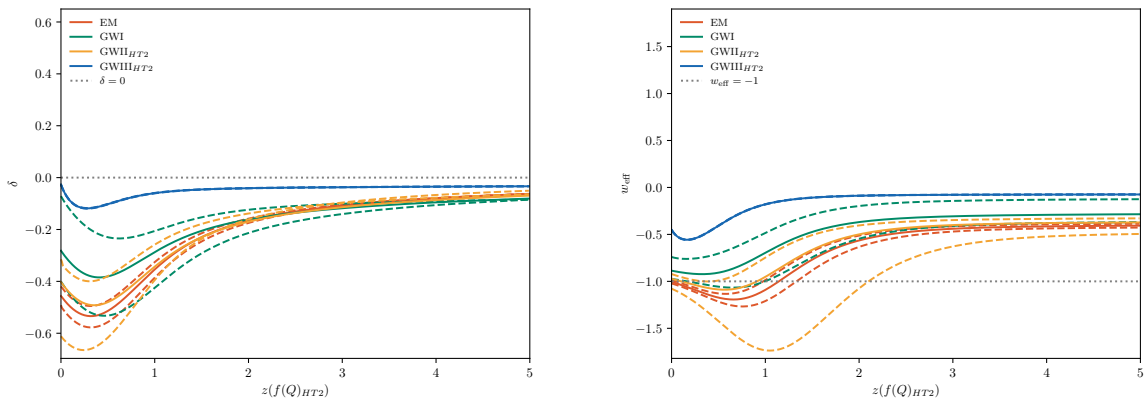


Fig. 8 Same as Fig. 6, but for the $f(Q)_{HT2}$ model.

20. M.X. Lin, M. Raveri, W. Hu, *Phys. Rev. D* **99**(4), 043514 (2019). DOI 10.1103/PhysRevD.99.043514
21. E. Di Valentino, A. Melchiorri, J. Silk, *Phys. Rev. D* **93**(2), 023513 (2016). DOI 10.1103/PhysRevD.93.023513
22. N. Lee, Y. Ali-Haïmoud, N. Schöneberg, V. Poulin, *Phys. Rev. Lett.* **130**(16), 161003 (2023). DOI 10.1103/PhysRevLett.130.161003
23. F.K. Anagnostopoulos, S. Basilakos, E.N. Saridakis, *Phys. Lett. B* **822**, 136634 (2021). DOI 10.1016/j.physletb.2021.136634
24. J. Ferreira, T. Barreiro, J.P. Mimoso, N.J. Nunes, *Phys. Rev. D* **108**(6), 063521 (2023). DOI 10.1103/PhysRevD.108.063521
25. B. Xu, H. Yu, P. Wu, *Astrophys. J.* **855**(2), 89 (2018). DOI 10.3847/1538-4357/aad12
26. R. Briffa, C. Escamilla-Rivera, J. Said Levi, J. Mifsud, N.L. Pullicino, *Eur. Phys. J. Plus* **137**(5), 532 (2022). DOI 10.1140/epjp/s13360-022-02725-4
27. A. Lewis, S. Bridle, *Phys. Rev. D* **66**, 103511 (2002). DOI 10.1103/PhysRevD.66.103511
28. M. Maggiore, *Gravitational Waves. Vol. 2: Astrophysics and Cosmology* (Oxford University Press, 2018)
29. W. Zhao, C. Van Den Broeck, D. Baskaran, T.G.F. Li, *Phys. Rev. D* **83**, 023005 (2011). DOI 10.1103/PhysRevD.83.023005
30. R.G. Cai, T. Yang, *Phys. Rev. D* **95**(4), 044024 (2017). DOI 10.1103/PhysRevD.95.044024
31. D.M. Scolnic, et al., *Astrophys. J.* **859**(2), 101 (2018). DOI 10.3847/1538-4357/aab9bb

32. C. Zhang, H. Zhang, S. Yuan, T.J. Zhang, Y.C. Sun, *Res. Astron. Astrophys.* **14**(10), 1221 (2014). DOI 10.1088/1674-4527/14/10/002
33. R. Jimenez, L. Verde, T. Treu, D. Stern, *Astrophys. J.* **593**, 622 (2003). DOI 10.1086/376595
34. M. Moresco, L. Verde, L. Pozzetti, R. Jimenez, A. Cimatti, *JCAP* **07**, 053 (2012). DOI 10.1088/1475-7516/2012/07/053
35. M. Moresco, L. Pozzetti, A. Cimatti, R. Jimenez, C. Maraston, L. Verde, D. Thomas, A. Citro, R. Tojeiro, D. Wilkinson, *JCAP* **05**, 014 (2016). DOI 10.1088/1475-7516/2016/05/014
36. X. Xu, A.J. Cuesta, N. Padmanabhan, D.J. Eisenstein, C.K. McBride, *Mon. Not. Roy. Astron. Soc.* **431**, 2834 (2013). DOI 10.1093/mnras/stt379
37. T. Delubac, et al., *Astron. Astrophys.* **574**, A59 (2015). DOI 10.1051/0004-6361/201423969
38. A. Font-Ribera, et al., *JCAP* **05**, 027 (2014). DOI 10.1088/1475-7516/2014/05/027
39. N.G. Busca, et al., *Astron. Astrophys.* **552**, A96 (2013). DOI 10.1051/0004-6361/201220724
40. L. Samushia, et al., *Mon. Not. Roy. Astron. Soc.* **429**, 1514 (2013). DOI 10.1093/mnras/sts443
41. D. Stern, R. Jimenez, L. Verde, M. Kamionkowski, S.A. Stanford, *JCAP* **02**, 008 (2010). DOI 10.1088/1475-7516/2010/02/008
42. C. Blake, et al., *Mon. Not. Roy. Astron. Soc.* **425**, 405 (2012). DOI 10.1111/j.1365-2966.2012.21473.x
43. E. Gaztanaga, A. Cabre, L. Hui, *Mon. Not. Roy. Astron. Soc.* **399**, 1663 (2009). DOI 10.1111/j.1365-2966.2009.15405.x
44. M. Moresco, *Mon. Not. Roy. Astron. Soc.* **450**(1), L16 (2015). DOI 10.1093/mnras/slv037
45. J. Simon, L. Verde, R. Jimenez, *Phys. Rev. D* **71**, 123001 (2005). DOI 10.1103/PhysRevD.71.123001
46. C.H. Chuang, Y. Wang, *Mon. Not. Roy. Astron. Soc.* **426**, 226 (2012). DOI 10.1111/j.1365-2966.2012.21565.x
47. W.J. Percival, et al., *Mon. Not. Roy. Astron. Soc.* **401**, 2148 (2010). DOI 10.1111/j.1365-2966.2009.15812.x
48. C. Blake, et al., *Mon. Not. Roy. Astron. Soc.* **418**, 1707 (2011). DOI 10.1111/j.1365-2966.2011.19592.x
49. F. Beutler, C. Blake, M. Colless, D.H. Jones, L. Staveley-Smith, L. Campbell, Q. Parker, W. Saunders, F. Watson, *Mon. Not. Roy. Astron. Soc.* **416**, 3017 (2011). DOI 10.1111/j.1365-2966.2011.19250.x
50. J.Z. Qi, S. Cao, M. Biesiada, X. Zheng, H. Zhu, *Eur. Phys. J. C* **77**(8), 502 (2017). DOI 10.1140/epjc/s10052-017-5069-1
51. Y. Zhang, H. Zhang, *Eur. Phys. J. C* **81**(8), 706 (2021). DOI 10.1140/epjc/s10052-021-09501-1
52. T.G.F. Li, *Extracting Physics from Gravitational Waves: Testing the Strong-field Dynamics of General Relativity and Inferring the Large-scale Structure of the Universe*. Ph.D. thesis, Vrije U., Amsterdam, Vrije U., Amsterdam (2013)
53. E. Belgacem, Y. Dirian, S. Foffa, M. Maggiore, *Phys. Rev. D* **97**(10), 104066 (2018). DOI 10.1103/PhysRevD.97.104066
54. A.G. Riess, W. Yuan, L.M. Macri, D. Scolnic, D. Brout, S. Casertano, D.O. Jones, Y. Murakami, G.S. Anand, L. Breuval, et al., *The Astrophysical journal letters* **934**(1), L7 (2022)
55. E. Di Valentino, et al., *Astropart. Phys.* **131**, 102605 (2021). DOI 10.1016/j.astropartphys.2021.102605
56. E. Abdalla, et al., *JHEAp* **34**, 49 (2022). DOI 10.1016/j.jheap.2022.04.002
57. M. Raveri, W. Hu, *Phys. Rev. D* **99**(4), 043506 (2019). DOI 10.1103/PhysRevD.99.043506
58. J. Beltrán Jiménez, L. Heisenberg, T. Koivisto, *Phys. Rev. D* **98**(4), 044048 (2018). DOI 10.1103/PhysRevD.98.044048
59. J. Beltrán Jiménez, L. Heisenberg, T.S. Koivisto, S. Pekar, *Phys. Rev. D* **101**(10), 103507 (2020). DOI 10.1103/PhysRevD.101.103507
60. L. Heisenberg, *Phys. Rept.* **1066**, 1 (2024). DOI 10.1016/j.physrep.2024.02.001
61. R. Lazkoz, F.S.N. Lobo, M. Ortiz-Baños, V. Salzano, *Phys. Rev. D* **100**(10), 104027 (2019). DOI 10.1103/PhysRevD.100.104027
62. I. Ayuso, R. Lazkoz, V. Salzano, *Phys. Rev. D* **103**(6), 063505 (2021). DOI 10.1103/PhysRevD.103.063505
63. S. Mandal, P.K. Sahoo, *Phys. Lett. B* **823**, 136786 (2021). DOI 10.1016/j.physletb.2021.136786
64. B.J. Barros, T. Barreiro, T. Koivisto, N.J. Nunes, *Phys. Dark Univ.* **30**, 100616 (2020). DOI 10.1016/j.dark.2020.100616
65. L. Atayde, N. Frusciante, *Phys. Rev. D* **104**(6), 064052 (2021). DOI 10.1103/PhysRevD.104.064052
66. J. Ferreira, (2023)
67. S. Nojiri, S.D. Odintsov, (2024)
68. S. Nojiri, S.D. Odintsov, *Phys. Dark Univ.* **45**, 101538 (2024). DOI 10.1016/j.dark.2024.101538
69. F. Bajardi, S. Capozziello, *Eur. Phys. J. C* **83**(6), 531 (2023). DOI 10.1140/epjc/s10052-023-11703-8
70. N. Frusciante, *Phys. Rev. D* **103**(4), 044021 (2021). DOI 10.1103/PhysRevD.103.044021
71. A. Paliathanasis, *Phys. Dark Univ.* **41**, 101255 (2023). DOI 10.1016/j.dark.2023.101255
72. H. Shabani, A. De, T.H. Loo, *Eur. Phys. J. C* **83**(6), 535 (2023). DOI 10.1140/epjc/s10052-023-11722-5
73. O. Sokoliuk, S. Arora, S. Praharaj, A. Baransky, P.K. Sahoo, *Mon. Not. Roy. Astron. Soc.* **522**(1), 252 (2023). DOI 10.1093/mnras/stad968
74. K. Flathmann, M. Hohmann, *Phys. Rev. D* **103**(4), 044030 (2021). DOI 10.1103/PhysRevD.103.044030

75. R. Solanki, A. De, P.K. Sahoo, *Phys. Dark Univ.* **36**, 100996 (2022). DOI 10.1016/j.dark.2022.100996
76. S. Capozziello, R. D'Agostino, *Phys. Lett. B* **832**, 137229 (2022). DOI 10.1016/j.physletb.2022.137229
77. S.A. Narawade, L. Pati, B. Mishra, S.K. Tripathy, *Phys. Dark Univ.* **36**, 101020 (2022). DOI 10.1016/j.dark.2022.101020
78. N. Dimakis, A. Paliathanasis, M. Roumeliotis, T. Christodoulakis, *Phys. Rev. D* **106**(4), 043509 (2022). DOI 10.1103/PhysRevD.106.043509
79. N. Myrzakulov, M. Koussour, A.H.A. Alfedeel, H.M. Elkhair, *Chin. J. Phys.* **86**, 300 (2023). DOI 10.1016/j.cjph.2023.10.001
80. L. Pati, S.A. Narawade, S.K. Tripathy, B. Mishra, *Eur. Phys. J. C* **83**(5), 445 (2023). DOI 10.1140/epjc/s10052-023-11598-5
81. W. Khylllep, J. Dutta, E.N. Saridakis, K. Yesmakhanova, *Phys. Rev. D* **107**(4), 044022 (2023). DOI 10.1103/PhysRevD.107.044022
82. M. Koussour, N. Myrzakulov, A.H.A. Alfedeel, A. Abebe, *PTEP* **2023**(11), 113E01 (2023). DOI 10.1093/ptep/ptad133
83. A. Oliveros, M.A. Acero, *Int. J. Mod. Phys. D* **33**(01), 2450004 (2024). DOI 10.1142/S0218271824500044
84. I.S. Albuquerque, N. Frusciante, *Phys. Dark Univ.* **35**, 100980 (2022). DOI 10.1016/j.dark.2022.100980
85. L. Atayde, N. Frusciante, *Phys. Rev. D* **107**(12), 124048 (2023). DOI 10.1103/PhysRevD.107.124048
86. T.B. Gonçalves, L. Atayde, N. Frusciante, *Phys. Rev. D* **109**(8), 084003 (2024). DOI 10.1103/PhysRevD.109.084003
87. L. Heisenberg, M. Hohmann, S. Kuhn, *JCAP* **03**, 063 (2024). DOI 10.1088/1475-7516/2024/03/063
88. S. Bahamonde, K.F. Dialektopoulos, C. Escamilla-Rivera, G. Farrugia, V. Gakis, M. Hendry, M. Hohmann, J. Levi Said, J. Mifsud, E. Di Valentino, *Rept. Prog. Phys.* **86**(2), 026901 (2023). DOI 10.1088/1361-6633/ac9cef
89. R. Ferraro, *AIP Conf. Proc.* **1471**, 103 (2012). DOI 10.1063/1.4756821
90. Y. Zhang, H. Li, Y. Gong, Z.H. Zhu, *JCAP* **07**, 015 (2011). DOI 10.1088/1475-7516/2011/07/015
91. A. Awad, W. El Hanafy, G.G.L. Nashed, E.N. Saridakis, *JCAP* **02**, 052 (2018). DOI 10.1088/1475-7516/2018/02/052
92. K. Bamba, C.Q. Geng, C.C. Lee, (2010)
93. A. Paliathanasis, J.D. Barrow, P.G.L. Leach, *Phys. Rev. D* **94**(2), 023525 (2016). DOI 10.1103/PhysRevD.94.023525
94. K. Bamba, C.Q. Geng, C.C. Lee, L.W. Luo, *JCAP* **01**, 021 (2011). DOI 10.1088/1475-7516/2011/01/021
95. S.B. Nassur, M.J.S. Houndjo, I.G. Salako, J. Tossa, (2016)
96. I.G. Salako, M.E. Rodrigues, A.V. Kpadonou, M.J.S. Houndjo, J. Tossa, *JCAP* **11**, 060 (2013). DOI 10.1088/1475-7516/2013/11/060
97. S. Nesseris, S. Basilakos, E.N. Saridakis, L. Perivolaropoulos, *Phys. Rev. D* **88**, 103010 (2013). DOI 10.1103/PhysRevD.88.103010
98. R.C. Nunes, S. Pan, E.N. Saridakis, *JCAP* **08**, 011 (2016). DOI 10.1088/1475-7516/2016/08/011
99. R.C. Nunes, *JCAP* **05**, 052 (2018). DOI 10.1088/1475-7516/2018/05/052
100. S. Basilakos, S. Nesseris, F.K. Anagnostopoulos, E.N. Saridakis, *JCAP* **08**, 008 (2018). DOI 10.1088/1475-7516/2018/08/008
101. W.S. Zhang, C. Cheng, Q.G. Huang, M. Li, S. Li, X.D. Li, S. Wang, *Sci. China Phys. Mech. Astron.* **55**, 2244 (2012). DOI 10.1007/s11433-012-4945-9
102. S. Capozziello, O. Luongo, R. Pincak, A. Ravanpak, *Gen. Rel. Grav.* **50**(5), 53 (2018). DOI 10.1007/s10714-018-2374-4
103. R.C. Nunes, S. Pan, E.N. Saridakis, *Phys. Rev. D* **98**(10), 104055 (2018). DOI 10.1103/PhysRevD.98.104055
104. R.C. Nunes, M.E.S. Alves, J.C.N. de Araujo, *Phys. Rev. D* **100**(6), 064012 (2019). DOI 10.1103/PhysRevD.100.064012
105. S.F. Yan, P. Zhang, J.W. Chen, X.Z. Zhang, Y.F. Cai, E.N. Saridakis, *Phys. Rev. D* **101**(12), 121301 (2020). DOI 10.1103/PhysRevD.101.121301
106. E. Jensko, (2024)
107. P. Wu, H.W. Yu, *Eur. Phys. J. C* **71**, 1552 (2011). DOI 10.1140/epjc/s10052-011-1552-2
108. F.K. Anagnostopoulos, V. Gakis, E.N. Saridakis, S. Basilakos, *Eur. Phys. J. C* **83**(1), 58 (2023). DOI 10.1140/epjc/s10052-023-11190-x
109. N.S. Kavya, S.S. Mishra, P.K. Sahoo, V. Venkatesha, *Mon. Not. Roy. Astron. Soc.* **532**, 3126 (2024). DOI 10.1093/mnras/stae1723
110. H. Akaike, *IEEE Trans. Automatic Control* **19**(6), 716 (1974). DOI 10.1109/TAC.1974.1100705
111. G. Schwarz, *Annals of Statistics* **6**(2), 461 (1978)